Journal of Structural Biology 171 (2010) 133–141

Contents lists available at ScienceDirect

Journal of Structural Biology

journal homepage: www.elsevier.com/locate/yjsbi

Moisture changes in the plant cell wall force cellulose crystallites to deform

S. Zabler [a,b,*], O. Paris [b,c], I. Burgert [b], P. Fratzl [b]

[a] Technische Universität Berlin – Werkstofftechnik, EB 13, Straße des 17. Juni 135, D-10623 Berlin, Germany
[b] Max-Planck Institute of Colloids and Interfaces, Department of Biomaterials, 14472 Potsdam, Germany
[c] Montanuniversität Leoben, Institut für Physik, Franz-Josef-Strasse 18, A-8700 Leoben, Austria

ARTICLE INFO

Article history:
Received 12 November 2009
Received in revised form 23 April 2010
Accepted 24 April 2010
Available online 8 May 2010

Keywords:
Wood cell wall
Cellulose
X-ray diffraction
Moisture
Humidity
Hydro-motility

ABSTRACT

Nano-crystallite deformation of cellulose microfibrils in the secondary cell wall layer of spruce wood tracheids was observed during de- and rehydration experiments below the fibre saturation point. A quantitative analysis of the (0 0 4), (2 0 0) and the (1 1 0)/(1 $\bar{1}$ 0) doublet X-ray diffraction peaks revealed longitudinal contraction, lateral expansion and changes in the monoclinic angle of the cellulose unit cell during drying of wood fibres. Experiments on unfixed samples as well as the simultaneous application of mechanical tensile and dehydration stress to samples hold at constant length showed two deformation mechanisms of different nature and magnitude. The first mechanism depends on the relative wood moisture content and the second one on the macroscopic tensile stress. These findings imply a new perspective on the role of water adsorption perceiving a hydration-induced structural change of cellulose crystal structure as a major driving force for deformation.

1. Introduction

In the plant kingdom moisture changes in cell walls are a well-utilised concept to generate organ movements. Remarkable examples are the opening of pine cones upon drying (Dawson et al., 1997), the hygro-sensitive bending of carrot umbels (Lacey, 1980) or the bending movements of wheat awns which provide motility to the seed dispersal unit (Elbaum et al., 2007).

From a materials science perspective these movements are particularly interesting as the deformation pattern is already established in the nanostructure of the cell walls during growth and a metabolism is not required for actuation. It is just the reversible swelling and shrinkage of the cell wall matrix substance due to moisture changes that allows for the substantial bending of the organs directed by the orientation of stiff cellulose fibrils in the cell walls (Burgert and Fratzl, 2009). However, it is not clear yet, whether an active shortening of cell walls can be generated just by the volume shrinkage of the hydrophilic matrix components or if specific water–cellulose interactions are necessary to generate the high internal stresses.

To address this question, we studied the nano-structural deformation of cellulose microfibrils in the secondary cell wall of wood fibres upon dehydration and rehydration. Wood tissues were taken as a model system, since the hygroscopic behaviour of wood cell walls is particularly well described (Skaar, 1988).

The secondary cell wall of wood is composed of three layers whereby the central and thickest layer (called S2) is most important for the mechanical performance of the tissue. The S2 layer in (dry) spruce wood tracheids contains approximately 50% wt. cellulose the rest being hemicelluloses and lignin. A significant volume fraction (~80%) of the cellulose is known to form crystalline microfibrils which have a lateral thickness of ~3 nm and a length of ~30 nm along the microfibril axis (Andersson et al., 2003). In the S2 layer these fibrils have been observed in the form of agglomerates which – in addition to the crystalline fibrils – contain non-crystalline cellulose and hemicelluloses (mostly glucomannan in case of softwoods) (Salmen and Fahlen, 2006). The remaining interspaces between the cellulose agglomerates are filled with a continuous matrix of lignin and hemicelluloses (mostly xylan). Cellulose agglomerates and matrix have been reported to group in concentric lamellae of approximately 20–30 nm repeat (Fahlén and Salmén, 2002). When moisture sorption is considered this non-crystalline part of the cellulose agglomerates is believed to bind most of the water which enters the cell wall.

The structure of crystalline cellulose has been investigated for a long time by means of X-ray and neutron diffraction (O'Sullivan, 1997; Kataoka and Kondo, 1999; Nishiyama et al., 2002, 2003). The native form of cellulose in wood contains two allomorph structures named Iα and Iβ, the latter being the dominant one (Atalla and VanderHart, 1984; Hult et al., 2000). Since the methods used in this work do not allow for distinguishing between these two

* Corresponding author at : Technische Universität Berlin – Werkstofftechnik, EB 13, Straße des 17. Juni 135, D-10623 Berlin, Germany. Fax: +49 (0)30 314 26673.
E-mail address: simon.zabler@tu-berlin.de (S. Zabler).

1047-8477/$ - see front matter © 2010 Elsevier Inc. All rights reserved.
doi:10.1016/j.jsb.2010.04.013

forms we will refer to the structural parameters of the Iβ form which have been determined to a monoclinic elementary cell of dimensions $a = 0.7784$ nm, $b = 0.8201$ nm with an angle $\gamma = 96.5°$ and $c = 1.0380$ nm, whereby c designs the longitudinal lattice spacing along the microfibril axis (Nishiyama et al., 2002). The size and arrangement of individual microfibrils has been studied by direct imaging methods (AFM and HRTEM; Näslund et al., 1988; Helbert et al., 1998; Imai et al., 2003; Baker et al., 1997) and by X-ray and neutron-small-angle scattering methods (Reiterer et al., 1998; Müller et al., 2000; Jungnikl et al., 2008; Astley and Donald, 2001). Cellulose microfibrils (i.e. their stiffness, microfibril angle, etc.) are decisive for the mechanical behaviour of single wood fibres and bulk wood (Fratzl et al., 2004; Müller et al., 2006; Rüggeberg et al., 2008). But also the structure–mechanical role of the hemicelluloses in the cell wall is a matter of ongoing discussion (Fratzl et al., 2004; Jungnikl et al., 2007).

Structural changes in wood which are due to changes in moisture have been studied for long on the micro- as well as on the macroscopic scale (Skaar, 1988; Treloar, 1953; Taniguchi, 1978; Jakob et al., 1996). The humidity point where the cell lumina are completely empty while the cell wall is still water-saturated is called the fibre saturation point X_{FS}. In terms of normal wood of spruce at 20 °C, X_{FS} is around 30% moisture content (Skaar, 1988, chapter 1.6). Below the fibre saturation point, anisotropic shrinkage or swelling is the most directly visible result of wood de- and rehydration, respectively. It is well known that the magnitude of deformation varies with tree species, wood density and the microfibrillar angle (MFA) (Skaar, 1988; Badel and Perre, 2002; Donaldson, 2008; Washusen et al., 2001). Structural changes in the cell walls, by means of rearrangement of cellulose fibrils due to dehydration were studied for flax and for spruce wood fibres using small angle X-ray scattering (SAXS) (Astley and Donald, 2001; Jakob et al., 1996). Recently, Abe and Yamamoto reported on deformation of cellulose microfibrils in Hinoki cypress induced by dehydration and hydrothermal treatment (Abe and Yamamoto, 2005, 2006). Shifts of the (0 0 4) and (2 0 0) diffraction peaks of crystalline cellulose revealed lateral expansion and longitudinal shrinkage of the microfibrils when wood was dehydrated (Abe and Yamamoto, 2005). A lateral expansion was also observed during the hydrothermal treatment but hardly any dimensional changes in the longitudinal direction were measured. Abe and Yamamoto explained this effect by a strong lateral compression of the cellulose crystals by the matrix substances in the green state (Abe and Yamamoto, 2006).

As yet, a complete picture of the triple interplay between mechanical stress, moisture and the structural changes of the cellulose microfibrils in plant cell walls is missing. The deformation of cellulose crystallites under macroscopic tensile stress has been reported (Peura et al., 2007), but the effect of simultaneous dehydration and tensile loading on the cellulose crystallites has not been investigated yet. Stress is known to change the water sorption properties of wood (below X_{FS}), because the cell wall can take up more water under tensile stress and less water under compressive stress (Treloar, 1953). Furthermore a dehydration stiffening was observed below X_{FS} (Peura et al., 2006). With this report we present new results which aim at differentiating the reactions of crystalline cellulose when either mechanical or dehydration stresses are applied. The cellulose structure is monitored in situ during dehydration and mechanical loading using synchrotron wide angle X-ray diffraction (XRD) on the μSpot beamline at the BESSY Synchrotron Berlin, Germany.

2. Materials and method

Longitudinal–tangential sheets of approximately 40 mm length, 3 mm width and 0.2 mm thickness were cut with a Leica microtom (RM2265) from never-dried spruce normal wood (*Picea abies* [L.] Karst). Normal wood was chosen because of its small microfibril angle (<10°). The sheets were fixed in an in situ tensile tester with an effective strain-length of ~30 mm by gluing (superglue Loctite 401) the samples ends between two thin plastic sheets (3 mm × 3 mm) and then fixing them in aluminium grips by tightening screws. The testing device was integrated into a sealed X-ray measurement chamber to allow for atmosphere control (temperature and relative air humidity RH).

After measuring the sorption isotherms of the material, RH could be scaled to X, the relative moisture content of wood in per cent which is defined as

$$X = 100 \cdot \frac{M - M_0}{M_0} \quad (1)$$

Here M is the weight of the wet wood at a given relative humidity RH and M_0 is the weight of the dry wood (see also Appendix B).

The full de- and rehydration processes were applied to four samples of spruce wood:

(i) Sample (1) was measured without confinement (zero stress),
(ii) Sample (2) was held at constant length applying a minimal pre-stress (100 kPa); after de- and rehydration the sample was loaded in a tensile test at constant humidity (wet condition) until fracture occurred,
(iii) Sample (3) was held at constant length and ~10 MPa pre-stress were applied, and
(iv) Sample (4) was held at constant length with ~19.1 MPa pre-stress applied before starting the measurement.

The X-ray diffraction measurements in transmission geometry were performed at the μSpot beamline at the BESSY II synchrotron radiation source, Berlin – Germany (Paris et al., 2007). Compared to conventional X-ray tubes, modern synchrotron facilities (in our case the BESSY facility in Berlin, Germany) deliver a highly intense, highly collimated and monochromatic X-ray beam which allows for recording diffraction patterns within seconds. The measurement chamber was mounted vertically with the sample surface facing the horizontal X-ray pencil beam. The beam-energy was monochromatized with a multilayer to yield an X-ray wavelength of 0.0775 nm. The beam diameter was set to 50 μm, thus enabling scanning across the tissue to avoid radiation damage as a result of long exposure times. The signal-to-noise ratio was substantially improved by applying 2 × 2 binning of the CCD based detector online during image acquisition. Typical exposure times were 1 or 2 s (see Fig. 1 for a typical example). After each exposure the sample was shifted horizontally along lines in 0.05 mm steps to avoid radiation damage by repeated exposure. For the same reason a vertical sample shift of 0.1 mm was applied after each row. A calibration of the q-axis ($q = 4\pi \sin\theta/\lambda$, with 2θ being the scattering angle and λ the wavelength) was done by comparison with a Corundum sample. Background intensities (caused by air scattering and Kapton foil) were removed by subtracting a reference frame taken without sample. Amorphous scattering contributions from the sample water were extrapolated from specific image regions (i.e. regions of the same q-interval which do not contain diffraction peaks, as it is for the example of the 2 0 0 peak indexed by the letter '$R_{[2\,0\,0]}$' in Fig. 1) and subtracted from the measured peak profiles. Radial and azimuthal integrations as well as fitting of the (0 0 4) and (2 0 0) peaks were performed with a customer-written software. Fitting of the (1 1 0) and (1 $\bar{1}$ 0) peaks with a double-Gaussian (of variable height and width) was done with the software QTIplot.[1] Since the microfibril orientation in the S2 cell wall of spruce

[1] QTIplot – Data Analysis and Scientific Plotting, ProIndep Serv S.r.l., Craiova, Romania.

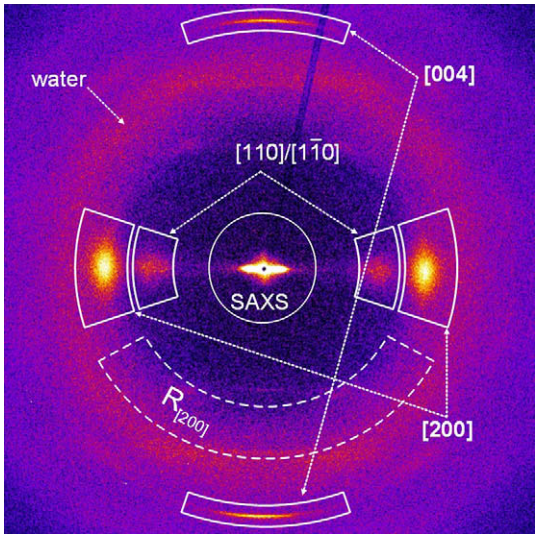

Fig. 1. Typical diffraction pattern of spruce normal wood fibres as recorded on the μSpot beamline at the BESSY synchrotron. While the small-angle scattering (SAXS) signal dominates the region close around the central beam, its broadening indicating the vertical orientation of the microfibrils, the outer image parts show multiple diffraction peaks from the crystalline cellulose elementary fibrils (indexed (0 0 4), (2 0 0) and (1 1 0/1 $\bar{1}$ 0)) as well as the broad amorphous scattering signal from the intracellular water. Peaks as well as the amorphous background signal were measured by angular integration, indicated by box segments. Additional segments (labelled with '*R*') were used to calculate the radial intensity of amorphous scatterers.

earlywood is almost parallel to the fibre long axis, two symmetrical peaks were analysed for each diffraction order. Their mean q-value was taken as the peak position to compensate for minor fluctuations of the X-ray beam centre.

Unlike comparable studies in which saturated salt solutions were used to adjust humidity (O'Brien, 1948; Greenspan, 1976), we employed a two-temperature humidity generator which uses pure water instead of salt solutions: RH can be adjusted continuously between 0% and 100% and equilibrium is reached within minutes (cf. Appendix A). The time periods needed for the wood to attain equilibrium with the surrounding atmosphere were estimated from tensile force measurements on samples which had gone through stress relaxation being held at a constant length: After each dehydration-step tensile stresses (σ) build-up typically reaching constant values after 20–30 min. Therefore a delay of 40 min was respected after changing the relative humidity (RH) and before starting the X-ray scan. The measurement chamber was constantly held at 22.4 °C.

During the de- and rehydration experiments, humidity was first decreased and later increased by steps of ca. 10% RH. For each point (σ, RH) 50–60 X-ray diffraction patterns were recorded, scanning over the entire sample width. Consequently, for each new (σ, RH) pair, the vertical sample position was slightly shifted to avoid radiation damage caused by repeated scanning over one spot. Lattice parameters for the crystallites a- and c-axis were determined from the symmetrical (2 0 0) and (0 0 4) reflections, respectively. The exact formula for calculating diffraction peaks in a monoclinic elementary cell is given by

$$|q_{hkl}| = \frac{2\pi}{\sin\gamma}\sqrt{\left(\frac{h}{a}\right)^2 + \left(\frac{k}{b}\right)^2 - \frac{2hk}{ab}\cos\gamma + \left(\frac{l}{c}\right)^2 \sin^2\gamma} \qquad (2)$$

$|q_{hkl}|$ is the length of the reciprocal lattice vector given by the mean peak position which is measured as a function of the wood moisture content X.

The cellulose crystal lattice spacings a, b and c and the monoclinic angle γ were thus evaluated as a function of stress and humidity. In addition to the (2 0 0) and (0 0 4) diffraction peaks, the double peak (1 1 0)/(1 $\bar{1}$ 0) was analysed for measuring γ and b. γ could be calculated from the spacing Δq between the (1 1 0) and (1 $\bar{1}$ 0) peaks in the diffraction patterns, whereas b was found from their absolute q-positions. A first-order expansion in $\cos\gamma$ of the square root in Eq. (2) yields (for $\gamma > 90°$):

$$\Delta q = |q_{1\bar{1}0}| - |q_{110}| \approx \frac{-4\pi\cos\gamma}{\sqrt{a^2+b^2}} \Rightarrow \gamma \approx arc\cot\left[\frac{\Delta q\sqrt{a^2+b^2}}{-4\pi}\right] \qquad (3)$$

Calculating the b-axis spacing with the same approximation ($|\cos\gamma| \ll 1$) as a function of the average q-peaks $\langle q\rangle = (|q_{1\bar{1}0}| + |q_{110}|)/2$ yields

$$\langle q\rangle \approx \frac{2\pi\sqrt{a^2+b^2}}{ab\sin\gamma} \Rightarrow b \approx \left[\left(\frac{\langle q\rangle\sin\gamma}{2\pi}\right)^2 - \frac{1}{a^2}\right]^{-1/2} \qquad (4)$$

Eq. (5) finally gives the a-spacing which is a function of q_{200} and γ according to

$$a = \frac{4\pi}{\sin\gamma\cdot q_{200}} \qquad (5)$$

Thus, the three lattice parameters a, b and γ are defined by a set of three coupled non-linear Eqs. (3)–(5) which were solved in a closed loop.

The degree of longitudinal shrinkage from wet to dry of segments of the tested samples was determined by making several consecutive images at high magnification and reassembling them into one. The longitudinal length in wet and dry was then measured using ImageJ software. Density was examined on the same sample segments by measuring their oven dry mass and wet volume.

3. Results

In the first experiment (sample (1)), one full dehydration and one full rehydration curve was measured without fixation of the sample (zero stress) at various humidity points between 0% and 100% RH. First, we studied the reaction of γ and b upon de- and rehydration. Resulting values of these two parameters are shown in Fig. 2. There are hardly any noticeable changes of b (with the exception of the first point which shows a slightly higher value of b, cf. Fig. 2b) whereas γ shows a monotonous decrease upon drying, which we chose to approximate by a linear regression (dashed line shown in Fig. 2a). The inset in Fig. 2a shows an example of the double peak fit. Error bars refer to the 95% confidence interval of the numerical peak fit.

$$\gamma(X) \approx \frac{X}{C_0} + \gamma_0 \qquad (6)$$

With $C_0 = 31\%$ and $\gamma_0 = 97.3°$ (±0.35°), X given in [%] and $\gamma(X)$ in [°]. The average value of the lattice b-spacing was 0.856 nm (±0.013). Note that during following experiments neither γ nor b showed significant changes when tensile stress was applied to the samples (2)–(4) without changing X. Thus, γ was approximated by Eq. (6) and b was assumed constant for all data points.

Secondly, lattice strains were calculated with respect to the a- and c-axis parameters of the initially wet sample (lattice constants were measured wet to be $a = 0.785$ nm and $c = 1.032$ nm) assuming $b = 0.856$ = const. and γ according to Eq. (6).[2] Fig. 3 shows

[2] Because of the weak signal (samples (3) and (4) were measured with half the exposure time) of the 1 1 0/1 $\bar{1}$ 0 double peaks, we decided that this assumption was more reliable than repeating the coupled numerical fit of a, b, c and γ.

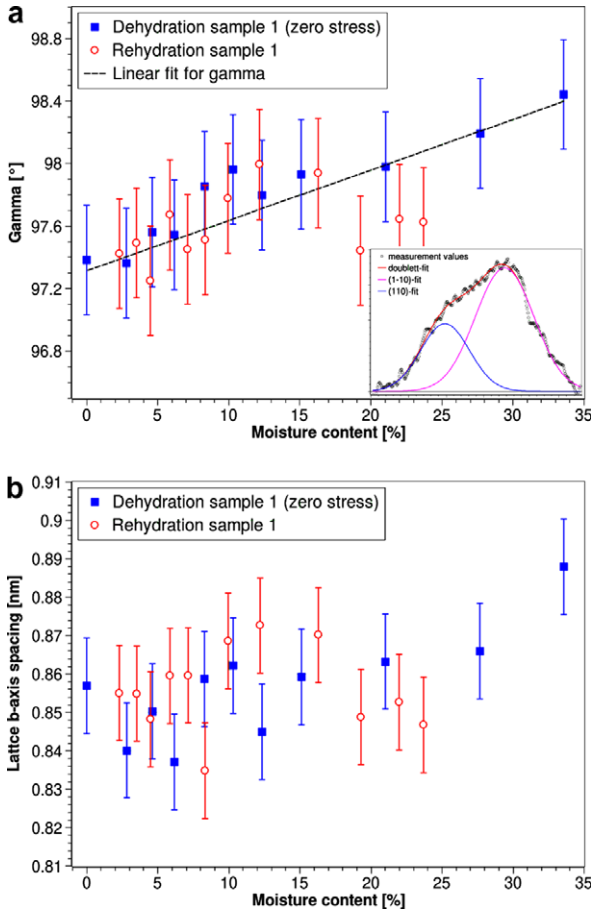

Fig. 2. Results of the iterative fit of the (1 1 0) and (1 $\bar{1}$ 0) double peak. The lattice spacing for the *b*-axis (a) and the monoclinic angle γ (b) are required for the correction of the *a*-axis spacing. During de- and rehydration $\gamma(X)$ is well approximated by a linear fit (dashed line) whereas no systematic changes are observed in the *b*-axis spacing. The latter is thus assumed constant. Note that fitting the double (1 1 0/1 $\bar{1}$ 0) peak is very delicate (inset) because of a major overlap and a generally very weak signal. Error bars refer to the 95% confidence intervals of the double peak fit and the resulting standard deviations of γ and *b*.

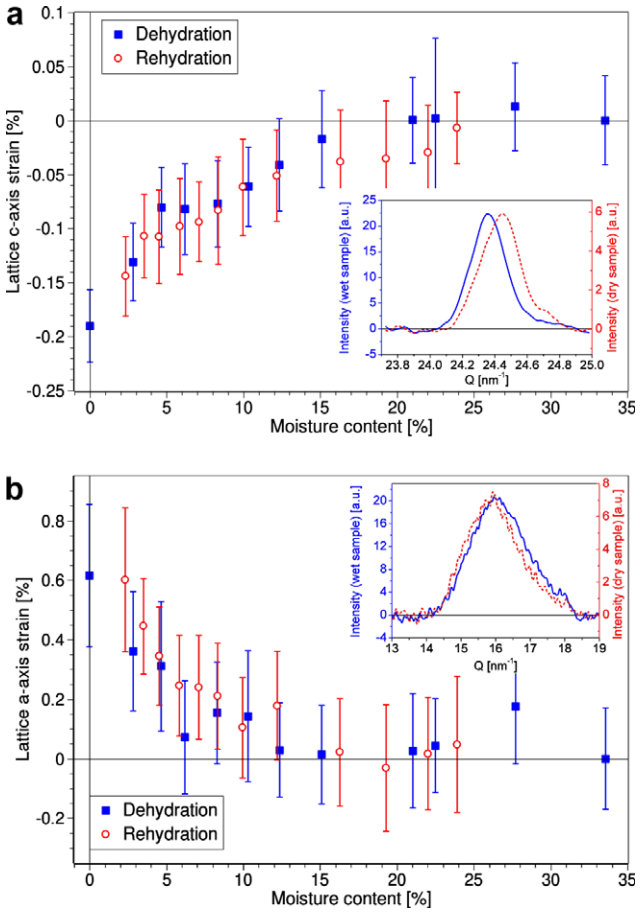

Fig. 3. (a) Evolution of the cellulose *c*-axis strain as a function of the sample moisture content *X*. Solid squares correspond to the dehydration of the unfixed (zero stress) sample (1) whereas the empty circles show the rehydration after drying the sample to $X = 0\%$. Error bars show the standard deviation of the peak position which is the average of 40–60 measurement points. (b) Evolution of the cellulose *a*-axis during de- and rehydration of the unfixed sample. Examples of the (0 0 4) and the (2 0 0) peak shifts from the wet (solid line) to the dry state (dashed line) is shown for single measurement points (insets in (a) and (b)).

the resulting evolution of strain in the crystallites *c*- and *a*-axis as a function of the moisture content *X* of sample (1). Error bars indicate the scattering of the lattice spacing which was derived from many diffraction patterns – a series of 50–60 diffraction patterns being taken over the entire sample width for every moisture value. Insets in Fig. 3a and b illustrate the peak shifts at individual measurement points between the wet and the dry state, from which the strains were calculated by $\varepsilon_a = (a(X)/a_{FS}) - 1$ and $\varepsilon_c = (c(X)/c_{FS}) - 1$, a_{FS} and c_{FS} being the corresponding reference lengths for the wet sample at the fibre saturation point. Note the slight skewness of both the (0 0 4) and (2 0 0) peaks. Along with a shift to smaller *q*-values the radial width of the (2 0 0) peak decreased slightly during dehydration whereas the (0 0 4) peak width did not show any change, possibly due to limited detector resolution. In parallel the scattered intensity of both (0 0 4) and (2 0 0) peaks decreased significantly. Dehydrating the sample from the fibre saturation point X_{FS} down to $X = 0\%$ caused the *a*-axis of the cellulose crystallites to expand by ~0.6% whereby the *c*-axis shortened by 0.2%. Rehydration reversed these strains precisely. Note that particularly for moisture contents below 10–15% the lattice parameters changed considerably while only weak fluctuations were observed between X_{FS} and 15%.

For the next sample (2), the de- and rehydration experiments were repeated while the sample was held at constant length in the testing device (zero strain). The sample was slightly pre-stressed in the wet state (100 kPa), and dehydration led to the build-up of internal tensile stresses reaching 7.9 MPa at the dry point (0% moisture content). A higher pre-stress (10 MPa) in the initially wet state was applied to the following sample (3) and the de-/rehydration cycle was repeated. Sample (3) reached 14.6 MPa total tensile stress at the dry point whereby significant changes in tensile stress and lattice parameters could only be noticed below 13% wood moisture. The highest pre-stress (19 MPa) was applied to the last sample (4) rising up to 22.1 MPa during dehydration. For sample (4) changes in tensile stress and lattice spacing could only be noticed below ~8% moisture content.

Fig. 4 summarises the measured tensile stresses plotted as functions of the *c*-axis (Fig. 4a) and *a*-axis (Fig. 4b) lattice spacing, as it evolved during de- and rehydration of the samples (1)–(4). Particularly for sample (2) (zero strain, minimal pre-stress) but also for samples (3) and (4) it can be clearly seen that the tensile stresses increase while the *c*-axis spacing is shortened due to dehydration. On the other hand the *c*-spacing values increase independently of the sample moisture content as a result of macroscopic stress. This effect can be observed for the wet and for the dry states ($X \sim 0\%$) of samples (1)–(4). After rehydration of samples (3) and (4), the remaining tensile stresses were relaxed and the structural parameters were measured once more (dashed arrows in Fig. 4 indicate

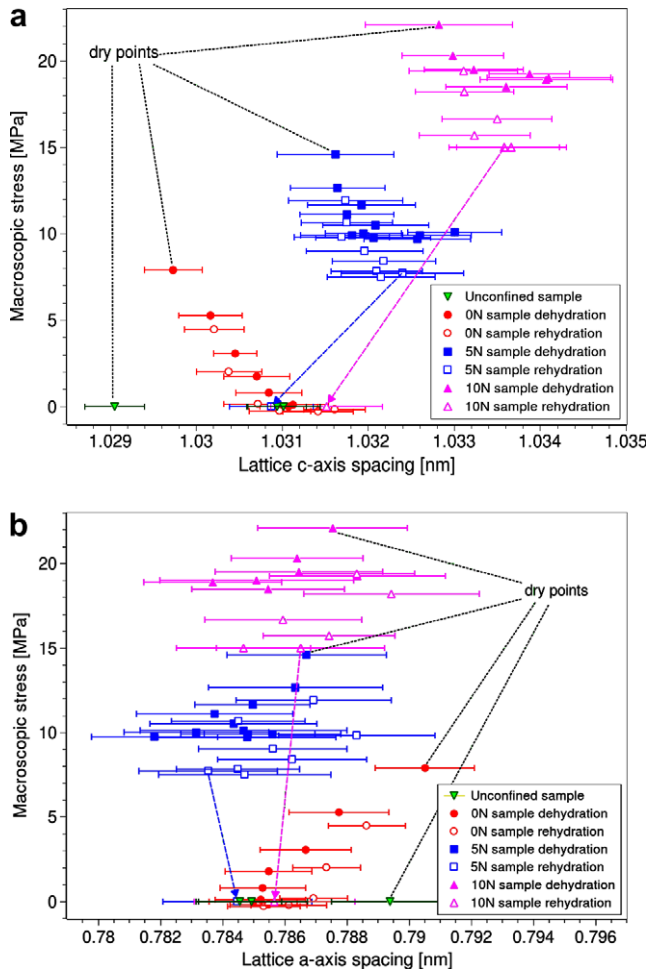

Fig. 4. (a) Evolution of the cellulose *c*-axis during simultaneous application of dehydration and tensile stress to samples (1)–(4). The dry points ($X = 0\%$) show the smallest *c*-axis spacing and the largest tensile stress. Mechanical relaxation after rehydration and sample release is shown by the dashed arrows for samples (3) and (4). Error bars show standard deviation of the peak position which is averaged from multiple measurement points. (b) Evolution of the cellulose *a*-axis during simultaneous application of dehydration and increasing tensile stress to samples (1)–(4).

this relaxation). The zero-stress *a*- and *c*-axis spacings for all four rehydrated samples are remarkably close to each other: 1.0309–1.0316 nm are found for the *c*-axis, 0.7845–0.7857 nm for the *a*-axis. Similar to Fig. 3b the lattice *a*-axis elongates during dehydration whereas it shortens during rehydration. No significant changes in the *a*-axis spacing are caused by tensile stress and/or relaxation (both dashed arrows in Fig. 4b are almost vertical) whereas a monotonous elongation of the *c*-axis is found upon tensile stress in the dry and the wet state, which relaxes when the samples are released. All findings are summarised in Table 1.

The full de- and rehydration cycles applied to the unfixed sample (1) and the fixed sample without pre-stress (sample (2)) reveal *q*-shifts in the (2 0 0) and (0 0 4) diffraction peaks indicating a significant lateral expansion of the crystallites in the *a*-axis (~0.6%) accompanied by a smaller longitudinal contraction (*c*-axis: ~−0.2%) upon dehydration. These values are considerably lower for the pre-stressed samples (3) and (4). For moisture contents above $X \sim 8$–13% the mechanical stress (and thus the longitudinal microstrain, cf. Fig. 4) applied to samples (3) and (4) appears to balance the dehydration induced longitudinal shrinkage of the fibrils (cf. Fig. 3). Shortening of the cellulose *c*-axis as well as lateral expansion accompanied by further (macro-)stress build-up during drying of samples (3) and (4) required moisture contents $X < 8$–13% to take effect. The dehydration induced microstrains were mostly reversible in the case of the unfixed sample (1) (cf. Fig. 3), whereas lower *q*-values of the (0 0 4) peak were measured after full rehydration of pre-stressed samples (3) and (4), compared to their initially wet state.

In order to evaluate the effect of tensile stress on the cellulose *a*- and *c*-axis, X-ray diffraction scans were taken during continuous tensile testing on sample (2) that had gone through the full cycle of de- and rehydration under minimal pre-stress and had reached $X \sim 28\%$ equilibrium moisture content. The sample was pulled at a constant strain-rate of 1 μm/s until fracture occurred at ~70 MPa tensile stress. Fig. 5a shows the macroscopic stress as a function of the lattice *c*-axis spacing (given by $c = 8\pi/q_{0\,0\,4}$) and Fig. 5b for the *a*-axis, respectively. From Fig. 5a a longitudinal deformation of the *c*-axis up to 0.3% (just before fracture) is clearly observed by the (0 0 4) peak shifts, whereby hardly any deformation occurs in the direction of the microfibrils' *a*-axis. The linear part of the (macro)stress–(micro)strain curve in Fig. 5a gives a modulus of 24 GPa (taking the total cross section of the sample). Note that the slope of this stress–strain curve is significantly higher than what was calculated from the dehydration induced stresses in Fig. 4a.

Our findings about the deformation of the unit cell in cellulose microfibrils induced by both dehydration and tensile straining are summarised in Fig. 6. Upon dehydration the crystal lattice of cellulose shortens in the longitudinal direction (−0.2%) and expands much more strongly in the transverse direction (0.6%). However, upon tensile straining a longitudinal elongation is observed which is in turn not accompanied by a measurable transverse contraction. Consequently, when wood is dried under load and/or held at constant length, a superposition of both the mechanical and the hygroscopic lattice deformations in cellulose microfibrils is observed. For moisture values below $X \sim 13\%$ the hygroscopic effects seem to be more important whereas for $X > 13\%$ the unit cell is mainly deformed by macroscopic tensile stresses.

4. Discussion

The deformation of cellulose nano-crystallites in the S2 layer was measured as a function of applied macroscopic tensile stress as well as upon de- and rehydration below the fibre saturation point. Our data indicate that both, mechanical stress-related and de-/rehydration-related deformation of the microfibrils coexist, but they have to be regarded as two distinct processes. The sign and ratio of lateral and longitudinal expansion and contraction of crystalline wood cellulose is thereby much different compared to

Table 1
Lattice spacing for the cellulose *a*- and *c*-axis measured under different stress–humidity conditions, as well as macroscopic tensile stress measured by a force transducer.

Sample no.	*a*[wet] (nm)	*a*[dry] (nm)	*a*[0 N] (nm)	*c*[wet] (nm)	*c*[dry] (nm)	*c*[0 N] (nm)	σ[wet] (MPa)	σ[dry] (MPa)	σ[reh] (MPa)
1	0.7846	0.7894	0.7849	1.0310	1.0291	1.0309	0	0	0
2	0.7850	0.7905	0.7855	1.0311	1.0297	1.0316	0.1	7.9	0
3	0.7847	0.7867	0.7845	1.0330	1.0316	1.0309	10	14.6	7.7
4	0.7837	0.7875	0.7857	1.0341	1.0328	1.0315	19.1	22.1	15

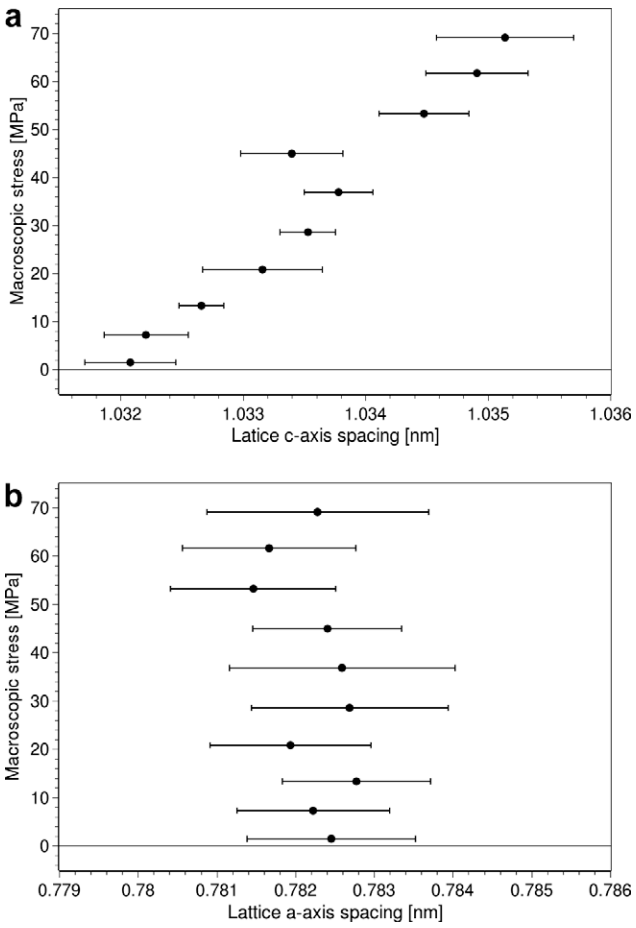

Fig. 5. (a) Deformation of the cellulose *c*-axis during continuous axial tensile testing. Error bars show the standard deviation of the peak position which is averaged from multiple (typically 40–60) diffraction measurements. The sample fractured shortly after reaching 70 MPa tensile stress. (b) Evolution of the cellulose *a*-axis.

the macroscopic effects observed during de- and rehydration of wood.

The (2 0 0), (1 1 0) and (1 $\bar{1}$ 0) diffraction peaks relate to the lattice spacing of the cellulose *a*- and *b*-axis as well as to the monoclinic angle γ. We showed that these three parameters are coupled via a set of three non-linear equations and appeared to be unaffected by macroscopic tensile stress. Within the precision of our measurement (particularly the signal of the (1 1 0) and (1 $\bar{1}$ 0) diffraction peaks was very weak) the *b*-axis was assumed constant for all data points and a linear decrease of γ with the sample moisture content was extrapolated for correcting the *a*-values. Our data is in agreement with findings by Langan et al. (2005) who did not observe dimensional changes in the *b*-axis upon temperature variations. Yet, it has to be noted that our measurement (*b* was mainly determined by the average (1 1 0) and (1 $\bar{1}$ 0) double-peak position $\langle q \rangle$) is not very sensitive to changes of *b* within the order of 1%, consequently conclusions have to be drawn with care.

We further observed (data not shown) the angular standard deviation (SD) of the (0 0 4) diffraction peak to decrease by ~1° (from 7.5° to 6.5°) during the first dehydration cycle of sample (1) but not during tensile testing at constant humidity. This small decrease may indicate a reorientation of the microfibrils during drying but is unlikely to add significantly to the lattice deformation since this gives a contribution of only 0.015% (1 − cos(1°)). For the standard deviation of the (2 0 0) peak no such increase was found. On the contrary, the peak SD was found to increase from 9° to 10° which could be the result of hygroscopic lateral distortion of the microfibrils. Unlike Evans (1999), who derived the microfibrillar angle (MFA) and its standard deviation from the angular peak profile of the (2 0 0) peak we were not able to determine the exact MFA value (because it was too small) and thus had to consider the angular widths as a mixture of constant MFA and stochastical misorientation of the fibrils.

From the (macro)stress–(micro)strain curve in Fig. 5a a modulus of 24 GPa was calculated on the basis of the total cross section of the sample. For the mechanically strained sample a density (dry weight/wet volume) of 0.249 g/cm^3 was measured. If we assume the volume fraction of cellulose to be 50% in the cell wall and the cellulose and cell wall density to be 1.5 g/cm^3, then a volume fraction of cellulose of 8% can be roughly calculated. A simple calculation of the elastic modulus of cellulose based on this volume fraction would lead to a value much higher than one could expect from literature (ca. 134 GPa) (Salmen, 2004) and would also exceed the elastic moduli that can be calculated from the hydration/dehydration experiments of the pre-stressed samples (Fig. 4). Therefore these findings show that the cellulose fibrils can not simply be treated as the exclusive load bearing component with fully elastic and homogenous deformation along their longitudinal axis. In fact, it is more reasonable to assume that shear stresses that are induced by the tensile loading cause the cellulose fibrils to slip (Keckes et al., 2003; Köhler et al., 2000; Altaner and Jarvis, 2008). An estimate of the microscopic shear-forces caused by the macroscopic longitudinal tensile stress would require knowledge of the exact MFA which was not available (see previous section).

Furthermore, strong stress relaxation was observed during de- and rehydration of the pre-stresses samples (2)–(4) due to the vis-

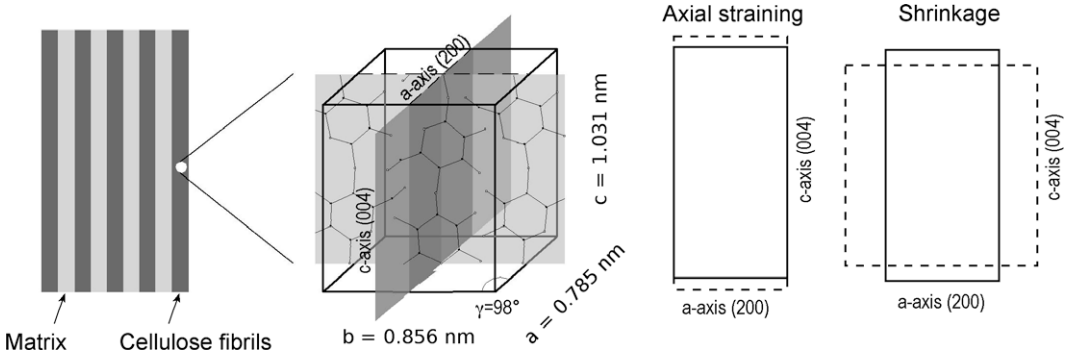

Fig. 6. Schematic drawing of the moisture and tensile loading induced deformation of the axial and lateral cellulose lattice parameters. During dehydration the *a*-axis expands by ~0.6% whereas the *c*-axis shortens by ~0.2%. The monoclinic angle decreases from ~98° to ~97° during dehydration whereas the *b*-axis which is parallel to the cellulose molecular sheets remains most likely stable at 0.856 nm. During axial tensile straining only the *c*-axis expands, whereas the *a*-axis remains almost constant.

co-elastic behaviour of wood. It has been shown that creep strain in wood is particularly pronounced when a sample is dehydrated under load (Armstrong and Kingston, 1962). Indeed slow relaxation processes were always observed when a sample was held (in our case for a time of ~40 min) at constant humidity and at constant length under stress. Consequently, comparing the (macro-)stress–(micro-)strain ratio in Fig. 4 to the tensile test in Fig. 5 is further problematic because creep effects are probably negligible for the 'fast' tensile experiment (Fig. 5) whereas they play an important role in the interpretation of Fig. 4.

The ratio of lattice deformation during hydration and dehydration experiments was measured to be $\varepsilon_c/\varepsilon_a = 0.3$ (0.2%/0.6%). However, this value does not display a Poisson's ratio, because the molecular deformation cannot be translated into the macroscopic concept of the interrelation of longitudinal and transverse strains. But the ratio indicates that the hygroscopic contraction along the cellulose *c*-axis can be the result of an anisotropic elastic deformation of the microfibrils. In the lateral plane the crystallites are build of hydrogen bonds and van der Waals linked glucose chains and their transverse Young modulus is rather low (ca. 27 GPa) whereas covalent bonds make the crystallites much stiffer along the *c*-axis (ca. 134 GPa) (Salmen, 2004). During the dehydration experiments, the lateral deformation of the crystallites might be strongly influenced by the interaction with water and/or matrix polymers. This is in agreement with the observed 'offset' of $X \sim 8$–13% above which no lattice deformation occurs in the pre-stressed samples (3) and (4). This phenomenon can be explained by reciprocal slipping of the microfibrils. From theory on creep deformation of wood it is known that under load the energy barrier against molecular slip is reduced which would explain that a certain amount of dehydration (and thus a sufficient cross linking of the matrix polymers) is needed to counter this 'slipping effect' (Smith et al., 2003).

Remarkably, the measured crystalline lattice expansion is an order of magnitude smaller and opposed to macroscopic lateral shrinkage (ca. 6–7% tangential shrinkage, depending on specimen size and composition (Skaar, 1988)) and therefore seems to be related to volume changes of matrix polymers, e.g. hemicelluloses which surround the microfibrils in the cellulose agglomerates. These findings agree qualitatively with Abe and Yamamoto who were the first to report on lateral expansion and longitudinal shrinkage of cellulose microfibrils upon drying (Abe and Yamamoto, 2005). Yet, they measured 1.51% lateral lattice strain during dehydration from $X = 25\%$ to $X = 5\%$ whereas lattice strains over the same moisture interval extrapolated from Fig. 3b were considerably lower. Abe and Yamamoto concluded from their results that the lateral expansion of the microfibrils is an elastic deformation caused by the swollen matrix which compresses the fibrils under wet and releases them under dry condition (Abe and Yamamoto, 2006). Although it is difficult to make a reliable estimate of the swelling pressure of the amorphous matrix, it seems unlikely that the matrix can generate a compressive stress of approximately 170 MPa which would be necessary to produce this magnitude of contraction (assuming a lateral stiffness of the cellulose crystals of 27 GPa). Furthermore, swelling of the amorphous cellulose segments is much more likely to deform the pliant hemicellulose/lignin matrix than the stiff microfibrils. Therefore, it seems unlikely that such high stresses are generated simply by the shrinkage of the matrix polymers due to drying.

Recent molecular mechanics simulations of native cellulose crystals in aqueous solution have shown the formation of multiple molecular layers of highly ordered compact water on the surface of cellulose microfibrils (Matthews et al., 2006). Such highly compact water (or ice) of extremely reduced mobility has also been reported experimentally on nanometre-sized hydrophilic surfaces and interfaces (Major et al., 2006; Tehei et al., 2007; Jinesh and Frenken, 2008). Knowing that the capillary condensation of water in nanoporous structures can induce strains as large as 0.5% in mesoprous silica ($E_{\text{Silica}} \approx 70$ GPa) (Prass et al., 2009), we think that similar processes might be responsible for the lateral expansion of the cellulose microfibrils upon moisture change. We hypothesise that the condensation and evaporation of ordered molecular layers of water (or a mixture of water, amorphous celluloses and hemicelluloses) on the hydrophilic surface of the microfibrils can create compressive stresses which are sufficient to shorten the lateral *a*-axis by ~0.6%. Consequently, during dehydration these compressive stresses are released and the lateral increase in length of the microfibrils is in direct contrast to the well-known macroscopic shrinkage of wood fibres and solid wood samples.

Acknowledgments

The financial support by the DFG (German Research Foundation) project: BU2132/1-1 is gratefully acknowledged. We thank Stefan Siegel, Chenghao Li, Markus Rüggeberg, Karin Jungnikl and Annemarie Martins for helpful support during sample preparation

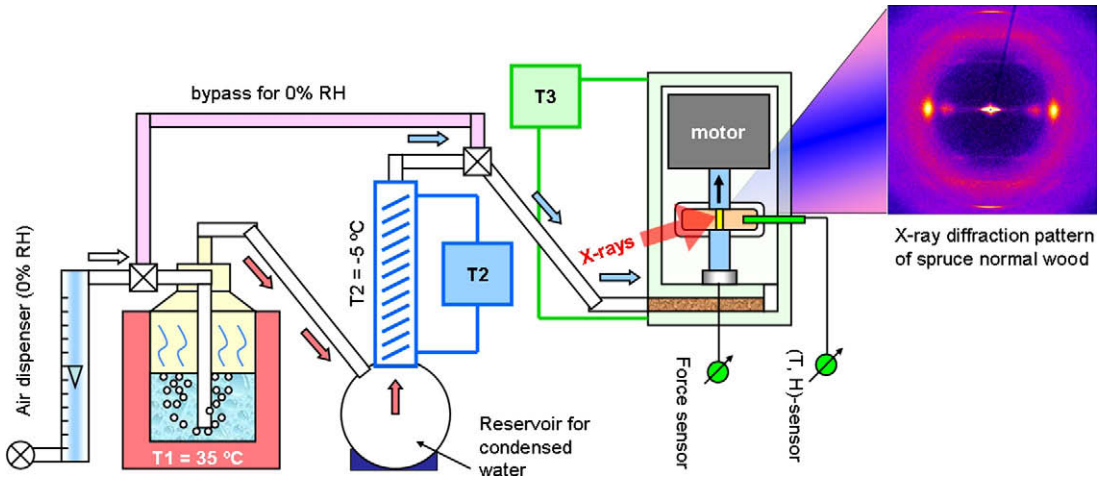

Fig. A1. Schematic drawing of the humidity control and measurement setup. From left to right: dry air from the dispenser is humidified by bubbling through hot water of temperature T_1, then water content is reduced by condensation in a cooler (temperature T_2). By adjusting T_2 the relative air humidity RH in the sample chamber (temperature $T_3 > T_2$) can be set precisely. The sample chamber comprises a vertical tensile tester onto which the sample is mounted with the wood tissues parallel to the direction of strain. A force sensor is connected to the bottom sample holder to measure tensile stress, the top holder is connected to a high precision linear motor. A 50 μm X-ray pencil beam traverses the two Kapton windows of the chamber and the 200 μm wood fibres. Wide angle diffraction patterns are recorded 30 cm downstream of the sample.

and BESSY beamtime (Helmholtz-Zentrum, Berlin für Materialien und Energie) experiments.

Appendix A. Humidity control and stress–strain measurements

The conventional method to adjust relative humidity in a closed sample chamber is to include a basin on the bottom which is then filled with various saturated salt solutions, each solution yielding specific equilibrium humidity in air (at constant temperature). This method has several drawbacks: (i) a large variety of salts is needed (some of which are harmful) to cover a significant range of humidity points between 0% and 100%; (ii) the smaller the interface between liquid solution and air, the longer the time until equilibrium is reached: hours sometimes days pass between two measurements, and (iii) changing humidity requires opening the chamber and changing the solution, thus for a short time the sample is exposed to ambient conditions which may influence the measurements.

As an alternative to saturated salt solutions we built a two-temperature humidity generator sketched in Fig. A1 (Buchczik and Ilewicz, 2001; Pohl et al., 2003; Lin and Chen, 2005). This system comprises three stages of different temperatures T_1, T_2 and T_3, the last one corresponding to the measurement chamber. For the temperature values the relation $T_1 \geqslant T_3 \geqslant T_2$ must be respected. First, dry air from a dispenser is bubbled through a wash bottle filled with warm (T_1 = 35 °C) distilled water thus humidifying the air to 100% RH. The wet air is then cooled down to a temperature T_2 reaching down to −15 °C in order to lower the dew point and to extract the excessive water by condensation. Downstream of the cooler, the air is led into the measurement chamber which – in our case – was operated at room temperature T_3 = 22.4 °C. Conveniently the relative humidity in the sample chamber can thus be adjusted continuously by changing T_2. Values between 13% RH (T_2 = −5 °C) and 100% RH ($T_2 = T_3$) have been used during the present work. Bypassing the system and introducing the dry air from the dispenser directly into the chamber yields ∼0% RH. T_3 and relative humidity were both measured inside the chamber using a Novasina Hygrodat-100 sensor system. With the exception of sample (1), the wood sheets were attached to two aluminium holders. The sample housing was mounted upright and strain was controlled by the top holder which connects to a PI (Physik-Instrumente) M-404 linear motor stage. Axial tensile forces were measured using a Honeywell R-30 load cell (50 N max. load), attached to the bottom holder.

Appendix B. Sorption isotherms

The wood moisture content X was measured as a function of relative air humidity H using the same type and size of samples and the humidifying system described previously. For this purpose the sample chamber was replaced by a Satorius ME 5 microbalance which was covered by a Plexiglas cylinder. The data was fitted using the one-hydrate model from Hailwood and Horrobin (1946)

Table B1
Coefficients found by fitting the measurement values to the one-hydrate model of Hailwood and Horobin along with literature values for de- and rehydration of spruce wood [456].

Source	M_p	K	K_1
First dehydration measured at 22.4 °C	155.553	0.657	1.470
First rehydration measured at 22.4 °C	330.890	0.808	4.154
Second dehydration measured at 22.4 °C	188.145	0.757	2.166
Literature Skaar'88: dehydration at 32 °C	221.948	0.741	11.02
Literature Skaar'88: rehydration at 32 °C	278.207	0.750	8.32

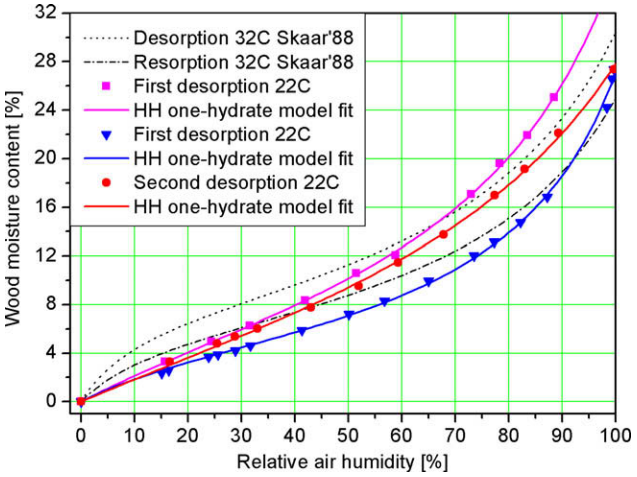

Fig. B1. Sorption isotherms measured with a Satorius microbalance SE 5 and the humidifying system sketched in Fig. A1. The measurement values for the first de- and rehydration as well as the values for the second rehydration (full hysteresis) were fitted by Eq. (2), the one-hydrate model of Hailwood and Horrobin (1946). Literature values from Ref. Skaar (1988) are shown as dotted/dashed lines.

$$X(\mathrm{RH}) = \frac{1800}{M_p} \cdot \left[\frac{K \cdot \mathrm{RH}}{100 - K \cdot \mathrm{RH}} + \frac{K_1 K \cdot \mathrm{RH}}{100 + K_1 K \cdot \mathrm{RH}} \right] \qquad \text{(B1)}$$

Here X and RH are given in per cent. The temperature dependent coefficients K, K_1 and M_p are shown in Table B1 for the first dehydration, rehydration and for the second dehydration cycle. Note that these values differ significantly from the literature values which are shown along in Table B1. This discrepancy might be due to the fact that the literature values were recorded at 32 °C whereas our experiment took place at 22 °C. Also larger samples comprising early- and latewood have probably been used whereas our sample was mainly earlywood. Fig. B1 shows the measured sorption isotherms for spruce normal wood along with two curves (dotted lines) corresponding to the literature values (Skaar, 1988). Note that due to experimental limitations the sorption isotherms could only be measured for an unfixed sample (zero stress equivalents sample (1)).

References

Abe, K., Yamamoto, H., 2005. Mechanical interaction between cellulose microfibril and matrix substance in wood cell wall determined by X-ray diffraction. J. Wood Sci. 51, 334–338.
Abe, K., Yamamoto, H., 2006. Change in mechanical interaction between cellulose microfibril and matrix substance in wood cell wall induced by hygrothermal treatment. J. Wood Sci. 52, 107–110.
Altaner, C.M., Jarvis, M.C., 2008. Modelling polymer interactions of the 'molecular Velcro' type in wood under mechanical stress. J. Theor. Biol. 253, 434–445.
Andersson, S., Serimaa, R., Paakkari, T., Saranpää, P., Pesonen, E., 2003. Crystallinity of wood and the size of cellulose crystallites in Norway spruce (*Picea abies*). J. Wood Sci. 49, 531–537.
Armstrong, L.D., Kingston, R.S.T., 1962. The effect of moisture content changes on the deformation of wood under stress. Austr. J. Appl. Sci. 13 (4), 257–276.
Astley, O.M., Donald, A.M., 2001. A small-angle X-ray scattering study of the effect of hydration on the microstructure of flax fibers. Biomacromolecules 2, 672–680.
Atalla, R.H., VanderHart, D.L., 1984. Native cellulose: a composite of two distinct crystalline forms. Science 223, 283–285.
Badel, E., Perre, P., 2002. Predicting oak wood properties using X-ray inspection: representation, homogenisation and localisation. Part 1: digital X-ray imaging and representation by finite elements. Ann. For. Sci. 59, 767–776.
Baker, A.A., Helbert, W., Sugiyama, J., Miles, M.J., 1997. High-resolution atomic force microscopy of native valonia cellulose I microcrystals. J. Struct. Biol. 119, 129–138.
Buchczik, D., Ilewicz, W., 2001. In: Fraczek, J. (Ed.), Proceedings of SPIE (2001). Optoelectronic and Electronic Sensors IV. pp. 106–109.
Burgert, I., Fratzl, P., 2009. Plants control the properties and actuation of their organs through the orientation of cellulose fibrils in their cell walls. Integr. Comp. Biol., 69–79.

Dawson, C., Vincent, J.F.V., Rocca, A., 1997. How pine cones open. Nature 390, 668.
Donaldson, L., 2008. Microfibril angle: measurement, variation and relationships – a review. IAWA J. 29, 345–386.
Elbaum, R., Zaltzman, L., Burgert, I., Fratzl, P., 2007. The role of wheat awns in the seed dispersal unit. Science 316, 884–886.
Evans, R., 1999. A variance approach to the X-ray diffractometric estimation of microfibril angle in wood. APPITA J. 52, 283.
Fahlén, J., Salmén, L., 2002. On the lamellar structure of the tracheid cell wall. Plant Biol. (Stuttg.) 4 (3), 339–345.
Fratzl, P., Burgert, I., Keckes, J., 2004. Mechanical model for the deformation of the wood cell wall. Z. Metallkd. 95, 1–6.
Greenspan, L., 1976. Humidity fixed points of binary saturated aqueous solutions. J. Res. N.B.S. A Phys. Chem. 81A (1), 89–96.
Hailwood, A.J., Horrobin, S., 1946. Absorption of water by polymers. Analysis in terms of a simple model. Trans. Faraday Soc. 42B. 84–92, 94–102.
Helbert, W., Nishiyama, Y., Okano, T., Sugiyama, J., 1998. Molecular imaging of *Halocynthia papillosa* cellulose. J. Struct. Biol. 124, 42–50.
Hult, E.-L., Larsson, P.T., Iversen, T., 2000. A comparative CP/MAS 13C-NMR study of cellulose structure in spruce wood and kraft pulp. Cellulose 7 (1), 35–55.
Imai, T., Putaux, J., Sugiyama, J., 2003. Geometric phase analysis of lattice images from algal cellulose microfibrils. Polymer 44, 1871–1879.
Jakob, H.F., Tschegg, S.E., Fratzl, P., 1996. Hydration dependence of the wood-cell wall structure in *Picea abies*. A small-angle scattering study. Macromolecules 29, 8435–8440.
Jinesh, K.B., Frenken, J.W.M., 2008. Experimental evidence for ice formation at room temperature. Phys. Rev. Lett. 101, 36101.
Jungnikl, K., Paris, O., Fratzl, P., Burgert, I., 2007. The implication of chemical extraction treatments on the cell wall nanostructure of softwood. Cellulose 15, 407–418.
Jungnikl, K., Koch, G., Burgert, I., 2008. A comprehensive analysis of the relation of cellulose microfibril orientation and lignin content in the S2 layer of different tissue types of spruce wood (*Picea abies* (L.) Karst.). Holzforschung 62, 475–480.
Kataoka, Y., Kondo, T., 1999. Quantitative analysis for the cellulose Ia crystalline phase in developing wood cell walls. Int. J. Biol. Macromol. 24, 37–41.
Keckes, J., Burgert, I., Frühmann, K., Müller, M., Kölln, K., Hamilton, M., Burghammer, M., Roth, S.V., Stanzl-Tschegg, S.E., Fratzl, P., 2003. Cell-wall recovery after irreversible deformation of wood. Nat. Mater. 2, 810–814.
Köhler, L., Speck, T., Spatz, H.C., 2000. Micromechanics and anatomical changes during early ontogeny of two lianescent Aristolochia species. Planta 210, 691–700.
Lacey, E.P., 1980. The influence of hygroscopic movement on seed dispersal in *Daucus carota* (Apiaceae). Oecologia 47, 110–114.
Langan, P., Sukumar, N., Nishiyama, Y., Chanzy, H., 2005. Synchrotron X-ray structures of cellulose Ib and regenerated cellulose II at ambient temperature and 100 K. Cellulose 12, 551–562.
Lin, S.X.Q., Chen, X.D., 2005. An effective laboratory air humidity generator for drying research. J. Food Eng., 125–131.
Major, R.C., Houston, J.E., McGrath, M.J., Siepmann, J.I., Zhu, X.-Y., 2006. Viscous water meniscus under nanoconfinement. Phys. Rev. Lett. 96, 177803.
Matthews, J.F. et al., 2006. Computer simulation studies of microcrystalline cellulose Ib. Carbohydr. Res. 341, 138–152.
Müller, M., Czihak, C., Burghammer, M., Riekel, C., 2000. Combined X-ray microbeam small-angle scattering and fibre diffraction experiments on single native cellulose fibres. J. Appl. Cryst. 33, 817–819.
Müller, M., Burghammer, M., Sugiyama, J., 2006. Direct investigation of the structural properties of tension wood cellulose microfibrils using microbeam X-ray fibre diffraction. Holzforschung 60, 474–479.
Näslund, P., Vuong, R., Chanzy, H., 1988. Diffraction contrast transmission electron microscopy on flax fiber ultrathin cross sections. Text. Res. J., 414–417.
Nishiyama, Y., Langan, P., Chanzy, H., 2002. Crystal structure and hydrogen-bonding system in cellulose Ib from synchrotron X-ray and neutron fiber diffraction. J. Am. Chem. Soc. 124, 9074–9082.
Nishiyama, Y., Sugiyama, J., Chanzy, H., Langan, P., 2003. Crystal structure and hydrogen bonding system in cellulose Ia from synchrotron X-ray and neutron fiber diffraction. J. Am. Chem. Soc. 125, 14300–14306.
O'Brien, F.E.M., 1948. The control of humidity by saturated salt solutions. J. Sci. Instrum. 25, 73–76.
O'Sullivan, A.C., 1997. Cellulose: the structure slowly unravels. Cellulose 4, 173–207.
Paris, O. et al., 2007. A new experimental station for simultaneous X-ray microbeam scanning for small- and wide-angle scattering and fluorescence at BESSY II. J. Appl. Cryst. 40, s466–s470.
Peura, M. et al., 2006. Negative Poisson ratio of crystalline cellulose in kraft cooked Norway spruce. Biomacromolecules 7, 1521–1528.
Peura, M. et al., 2007. The effect of axial strain on crystalline cellulose in Norway spruce. Wood Sci. Technol. 41, 565–583.
Pohl, M., Karižˇ, Z., Bajsić, I., 2003. In: XVII IMEKO World Congress Proceedings. Dubrovnik, Croatia, pp. 1642–1645.
Prass, J., Müter, D., Fratzl, P., Paris, O., 2009. Capillarity-driven deformation of ordered nanoporous silica. Appl. Phys. Lett. 95, 083121.
Reiterer, A., Jakob, H.F., Stanzl-Tschegg, S.E., Fratzl, P., 1998. Spiral angle of elementary cellulose fibrils in cell walls of *Picea abies* determined by small-angle X-ray scattering. Wood Sci. Technol. 32, 335–345.
Rüggeberg, M. et al., 2008. Stiffness gradients in vascular bundles of the palm *Washingtonia robusta*. Proc. R. Soc. B 275, 2221–2229.
Salmen, L., 2004. Micromechanical understanding of the cell-wall structure. C. R. Biol. 327, 873–880.
Salmen, L., Fahlen, J., 2006. Reflections on the ultrastructure of softwood fibers. Cell. Chem. Technol. 40, 181–185.
Skaar, C., 1988. Wood–Water Relations. Springer-Verlag, Berlin, Heidelberg, New York.
Smith, I., Landis, E., Gong, M., 2003. Fracture and Fatigue in Wood. John Wiley & Sons Ltd..
Taniguchi, T., 1978. Determination of water adsorption sites in wood by a hydrogen–deuterium exchange. Nature 272, 230–231.
Tehei, M. et al., 2007. Neutron scattering reveals extremely slow cell water in a Dead Sea organism. PNAS 104, 766–771.
Treloar, L.R.G., 1953. The absorption of water by cellulose, and its dependence on applied stress. Trans. Faraday Soc. 49, 816–823.
Washusen, R., Ades, P., Evans, R., Ilic, J., Vinden, P., 2001. Relationships between density, shrinkage, extractives content and microfibril angle in tension wood from three provenances of 10-year-old *Eucalyptus globulus* Labill. Holzforschung 55, 176–182.